Journal of Magnetic Resonance 200 (2009) 321–327

Contents lists available at ScienceDirect

Journal of Magnetic Resonance

journal homepage: www.elsevier.com/locate/jmr

Flat RF coils in static field gradient nuclear magnetic resonance

H. Stork [a,*], A. Gädke [a], N. Nestle [b], F. Fujara [a]

[a] Institut für Festkörperphysik, TU Darmstadt, Hochschulstraße 6, 64289 Darmstadt, Germany
[b] BASF SE Ludwigshafen, GKP/R 67056 Ludwigshafen, Germany

ARTICLE INFO

Article history:
Received 28 May 2009
Revised 11 July 2009
Available online 18 July 2009

Keywords:
SFG
Flat coil
Microimaging
STRAF1

ABSTRACT

The use of flat RF coils allows considerable gains in the sensitivity of static field gradient (SFG) nuclear magnetic resonance (NMR) experiments. In this article, this effect is studied theoretically as well as experimentally. Additionally, the flat coil geometry has been studied theoretically depending on magnetic field gradient, pulse sequence and amplifier power. Moreover, detecting the signal directly from the free induction decay (FID) turned out to be quite attractive for STRAFI-like microimaging experiments, especially when using flat coils. In addition to wound rectangular flat coils also spiral flat coils have been developed which can be manufactured by photolithography from printed circuit boards.

1. Introduction

Magnetic field gradients are widely used in NMR to achieve spatial resolution and also for diffusion studies. For this purposes static field gradients (SFG) are applied as well as pulsed field gradients (PFG). Both in standard magnetic resonance imaging (MRI) [1] and in NMR diffusometry (PFG–NMR, DOSY) [2–7], pulsed magnetic field gradients are used. While the pulsed field gradient approach offers advantages with respect to signal/noise ratio (SNR) the available gradient strengths are typically considerably lower than those available in static magnetic field gradients.

Furthermore, the gradient switching time of typically some hundred microseconds restricts the use of PFG–NMR to samples with relatively long spin–spin relaxation times (T_2)—mostly liquids. Solids, typically exhibiting short T_2 and low diffusion coefficient (D), can usually only be investigated by means of SFG NMR [8]. As large gradient strengths and short echo times are needed both for measuring small D and for spatially selective NMR excitation at short length scales, SFG NMR diffusometry [9–11] and strayfield NMR imaging (STRAFI) [12,13,9,14] are the only appropriate experimental options for such materials. For SFG NMR, magnetic field gradients of about 70 T/m can be achieved in the stray field of conventional superconducting NMR magnets, larger gradients can be realized in dedicated gradient magnet systems [15,10].

In this contribution, we present an approach to improve the SNR in SFG NMR by the use of flat RF coils. Flat RF coils are already used in high-resolution NMR [16,17]. Here, their advantages in SFG NMR will be discussed.

A major reason for the low SNR in SFG NMR is that only a thin slice of the sample can be excited due to limited bandwidth even of "hard" RF pulses. Therefore, it appears to be straightforward to increase the signal filling factor of the coil by using RF coils which contain less non-excited volume. But not only the signal filling factor changes when a solenoid coil with circular cross-section is replaced by a flat coil. Also the inductivity, the coil coefficient and a couple of additional parameters change. These effects are going to be reviewed in the next section and a quantitative derivation based on first principles will developed. After that, we will compare experimental signal intensities with calculated ones and thereby test our theoretical concept. In the next step, this approach is applied to optimize the coil geometry numerically. Finally, based on the results, possible benefits from flat coil designs for the SNR in SFG NMR are reviewed.

2. Theory

In order to calculate the NMR signal of flat coils their RF field has to be known. As long as the coil structures are small compared to the wave length, the RF field can be written in the form $\vec{B}_1(\vec{r},t) = f(t)\cdot\vec{B}_{stat}(\vec{r})$, where $\vec{B}_{stat}$ is the magnetic field a DC current of the same amplitude would produce. $\vec{B}_{stat}$ can be determined using the Biot–Savart law

$$\vec{B}_{stat}(\vec{r}') = \frac{\mu_0 I}{4\pi}\oint\frac{(\vec{r}-\vec{r}')\times d\vec{s}}{|\vec{r}-\vec{r}'|^3} \tag{1}$$

with I denoting the current and $d\vec{s}$ the line element along the coil windings. The inductivity L of the coil is given by

$$L = \frac{1}{I}\int\int\vec{B}_{stat}\cdot d\vec{f} = \frac{1}{I}\oint\vec{A}\cdot d\vec{s} \tag{2}$$

where $d\vec{f}$ is the surface element and $\vec{A}$ the vector potential.

* Corresponding author.
E-mail address: holgerstork@gmx.de (H. Stork).

1090-7807/$ - see front matter © 2009 Elsevier Inc. All rights reserved.
doi:10.1016/j.jmr.2009.07.018

Since in general the inductivity is the limiting factor for the implementation of a RF coil in a tank circuit of a given resonance frequency f_0, flat coils with similar L values but different thicknesses h were manufactured for the experimental studies, and in the theoretical studies of the NMR response as a function of slice thickness L was kept constant.

The starting point for the calculation of NMR signals is the induction law:

$$U_{ind} = -\frac{\delta}{\partial t}\int\int \vec{B}\cdot d\vec{f} \tag{3}$$

Transforming the area integral to a line integral, inserting the vector potential $\vec{A}$ of a magnetization distribution $\vec{M}(\vec{r},t)$ and changing the order of the line- and the volume integral yields, analogous to [18]

$$\begin{aligned} U_{ind} &= -\frac{\partial}{\partial t}\oint \vec{A}\cdot d\vec{s} = -\frac{\partial}{\partial t}\oint\iiint \frac{\mu_0}{4\pi}\frac{\vec{M}\times(\vec{r}-\vec{r}')}{|\vec{r}-\vec{r}'|^3}d^3r'd\vec{s} \\ &= -\frac{\partial}{\partial t}\iiint \vec{M}\cdot\underbrace{\frac{\mu_0}{4\pi}\oint\frac{(\vec{r}-\vec{r}')\times d\vec{s}}{|\vec{r}-\vec{r}'|^3}}_{\vec{b}_1}d^3r' \end{aligned} \tag{4}$$

A comparison to Eq. (1) indicates that the line integral term in Eq. (4) can be summarized as $\vec{b}_1(\vec{r}) = \frac{\vec{B}_1(\vec{r},t)}{I(t)}$ is the magnetic field of the coil divided by the current. In consistency with the principle of reciprocity [19], $\vec{b}_1(\vec{r})$ is nothing else than the coil coefficient of the RF coil. The integrand in Eq. (4) can be defined as signal density

$$u(\vec{r},t) = \dot{\vec{M}}(\vec{r},t)\cdot\vec{b}_1(\vec{r}) \tag{5}$$

In the following, $\dot{\vec{M}}(\vec{r},t)$ will be determined. Since this work focuses on the sensitivity of the RF coil, the sample properties and the NMR pulse sequences have been chosen such that dipolar couplings, relaxation and diffusion effects can be neglected. Additionally it is assumed that the RF field is constant within the coil and collinear to the x-axis $\vec{b}_1 = b_1(\vec{r}=\vec{0})\vec{e}_x$ and that the resonance frequency varies only according to a linear magnetic field gradient along the z-axis $\omega_0 = \omega_{ref} + \gamma G z$ shall be assumed, where ω_{ref} is the reference frequency, γ the gyromagnetic ratio and G the magnetic field gradient. In this case, the spin dynamics in the rotating coordinate system can be described by the Bloch equations [20] in matrix form

$$\dot{\vec{M}} = H\vec{M} \quad\Rightarrow\quad \vec{M}(t) = e^{Ht}\vec{M}_0 \tag{6}$$

where H is a matrix which depends on the frequency offset $\Delta\omega(z) = \gamma G z$ (gradient G and distance z) and the Larmor frequency due to the RF field[1] $\omega_1 = \frac{1}{2}\gamma I b_1$.

$$H = \begin{pmatrix} 0 & -\Delta\omega & 0 \\ \Delta\omega & 0 & -\omega_1 \\ 0 & \omega_1 & 0 \end{pmatrix} \tag{7}$$

When $\omega_1 = 0$ (in this case H := H_E) [21],

$$e^{H_E\tau} = \begin{pmatrix} \cos(\Delta\omega\cdot\tau) & -\sin(\Delta\omega\cdot\tau) & 0 \\ \sin(\Delta\omega\cdot\tau) & \cos(\Delta\omega\cdot\tau) & 0 \\ 0 & 0 & 1 \end{pmatrix} \tag{8}$$

and during the RF pulse ($H := H_P$) [21],

$$e^{H_P t_P} = \begin{pmatrix} \frac{\cos(\omega_{eff}\cdot t_P)\Delta\omega^2+\omega_1^2}{\omega_{eff}^2} & -\frac{\Delta\omega\cdot\sin(\omega_{eff}\cdot t_P)}{\omega_{eff}} & -\frac{(\cos(\omega_{eff}\cdot t_P)-1)\Delta\omega\cdot\omega_1}{\omega_{eff}^2} \\ \frac{\Delta\omega\cdot\sin(\omega_{eff}\cdot t_P)}{\omega_{eff}} & \cos(\omega_{eff}\cdot t_P) & -\omega_1\cdot\frac{\sin(\omega_{eff}\cdot t_P)}{\omega_{eff}} \\ -\frac{(\cos(\omega_{eff}\cdot t_P)-1)\Delta\omega\cdot\omega_1}{\omega_{eff}^2} & \omega_1\cdot\frac{\sin(\omega_{eff}\cdot t_P)}{\omega_{eff}} & \frac{\cos(\omega_{eff}\cdot t_P)\omega_1^2+\Delta\omega^2}{\omega_{eff}^2} \end{pmatrix} \tag{9}$$

with $\omega_{eff} = \sqrt{\omega_1^2+\Delta\omega^2}$.

[1] The factor ½ is due to the transformation of the RF field into the rotating frame (cf. [4]).

The magnetization response after the application of any pulse sequence then can be computed as the result of the subsequent application of the appropriate e^{Ht} operators.

Like that, we obtain the response after a single pulse as $\vec{M} = e^{H_E t_d}e^{H_P t_P}\vec{M}_0$ with t_d denoting the running signal acquisition time, and t_P the pulse length. For a Hahn echo with echo time τ we find

$$\vec{M} = e^{H_E\tau}e^{H_P(2\cdot t_P)}e^{H_E\tau}e^{H_P t_P}\vec{M}_0$$

Normally, the initial magnetization $\vec{M}_0$ is the equilibrium magnetization $\vec{M}_{eq} = \chi\cdot\vec{B}_0$ where χ is the magnetic susceptibility of the nuclear spins in the sample.

In order to calculate U_{rec}, the voltage recorded by the transient recorder, the magnetization has to be transformed into the laboratory system first. To enable a better distinction, from hereon the magnetization in the rotating frame shall be denoted as $\vec{M}^{rot}$.

Transforming back to the laboratory systems leads to a local contribution to the NMR signal intensity of

$$\begin{aligned} u(z,t) = b_1\cdot\Big(&\cos(\omega_{ref}t)\cdot\dot{M}_x^{rot} - \sin(\omega_{ref}t)\cdot\dot{M}_y^{rot} - \sin(\omega_{ref}t) \\ &\cdot\omega_{ref}\cdot M_x^{rot} - \cos(\omega_{ref}t)\cdot\omega_{ref}\cdot M_y^{rot}\Big) \end{aligned} \tag{10}$$

After mixing the signal with the reference frequency and filtering out the high-frequency contributions, this yields

$$u(z,t) = \frac{1}{2}b_1\left(\dot{M}_x^{rot} - \omega_{ref}M_y^{rot}\right) = -\frac{1}{2}b_1\omega_0 M_y^{rot} \tag{11}$$

The recorded voltage U_{rec} can be obtained by integration of Eq. (11) weighted with a spectrometer function f_{spec}, containing the resonance curve and the receiver characteristics:

$$U_{rec} = -l\cdot b\int u(z,t)\cdot f_{spec}(\Delta\omega(z))dz \tag{12}$$

The dimensions b and l are defined in Fig. 1. This integral has been solved numerically using [22].

3. Experimental

Seven different flat coils were tested. Six of them were rectangular flat coils (RFC) and one was a spiral flat coil (SFC) (see Fig. 1). As a reference, also a conventional solenoidal RF coil with circular cross-section was tested, too.

As sample water was used. In order to reduce the measurement time, it was doped with 0.04 M $CuSO_4$ which lead to a spin–lattice relaxation time T_1 of about 40 ms. The ^{1}H-Larmor frequency was 161.8 MHz.

The RFCs were wound directly around the sample containers. The sample containers were built from a rectangular ^{1}H free spacer frame made of DURATEC® (Cape Boards Siborit GmbH, Lüneburg, Germany) onto which 0.15 mm glass plates were glued on both sides. Filling was achieved through a tiny hole with a syringe needle. After filling the hole was sealed with a piece of Teflon as a plug. In order to eliminate the possibility of water loss after sample preparation the filling levels of the coils have been inspected directly before and after the measurement.

The thicknesses h of the RFCs were varied as well as their areas $l\times b$ perpendicular to the magnetic field gradient. The RFCs were wound manually from lacquer isolated copper band of 35 μm thickness. Therefore all dimensions vary by several tenths of millimeters. For this reason, it was practically not feasible to produce RFCs with $h < 2$ mm. By contrast, such small coil thicknesses could be easily realized for SFCs. A SFC consists of two electrically parallel spiral coils with opposite direction of turns. The spiral coils are connected in the center and at the edge (see Fig. 1). Since SFCs can be etched from printed circuits, a precision of better than

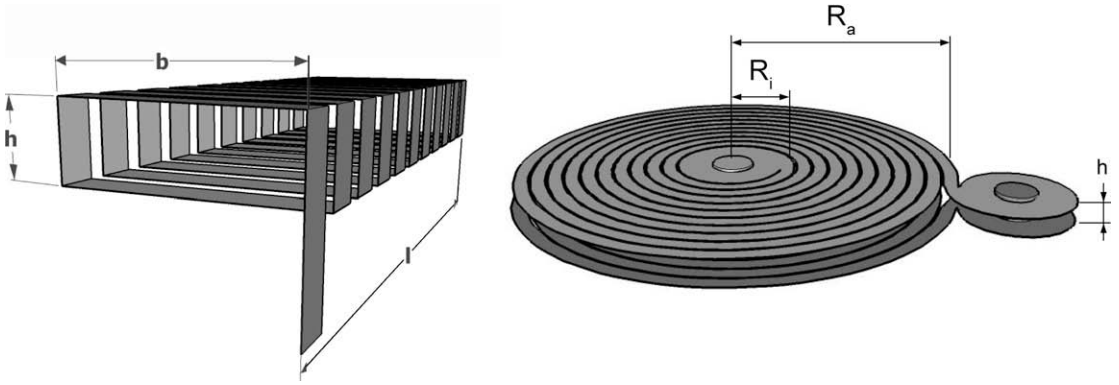

Fig. 1. Sketch of a rectangular (left) and a spiral flat coil (right). For the sake of clarity only the current leading components are shown. Structural materials which provide mechanical support to the coils are omitted.

50 μm is reached. SFCs are intrinsically less sensitive than comparable RFCs but they can be manufactured with smaller h.

An overview about all flat coils can be found in Table 1. In addition to the measured dimensions of the coils, Table 1 also provides the measured inductivities, the quality factors Q of the tank circuits and the calculated RF coil sensitivities. The inductivities L were experimentally determined by incorporating them into a parallel resonant circuit with a known capacity (C_r = 9.65 nF). Using a network analyser, the resonance frequencies f_r and resonance widths Δf_r were measured and the inductivities were calculated according to $L = \frac{1}{\pi^2(4f_r^2+\Delta f_r^2)\cdot C_r}$. The inductivities L_M of the matching coils (see Fig. 2) were determined in the same way.

Since the induction voltage U_{ind} was not measured directly, it was calculated using the measured voltage U, the inductivities L and L_M, the reference frequency ω_{ref} and the impedance Z of the coaxial cable:

$$U_{ind} = U \cdot \omega_{ref} L \cdot \sqrt{\frac{1}{Z^2} + \frac{1}{\omega_{ref}^2 L_M^2}} \tag{13}$$

The NMR measurements were done in the stray field of a dedicated superconducting gradient magnet (Magnex Scientific Ltd., Abingdon, UK) [10], in 97 mm distance from the center of the magnet, at a field of 3.8 T and a field gradient of 74 T/m. At this position the isolines of the magnetic field are flat (see Fig. 3). This is of great importance for the test measurements, because otherwise

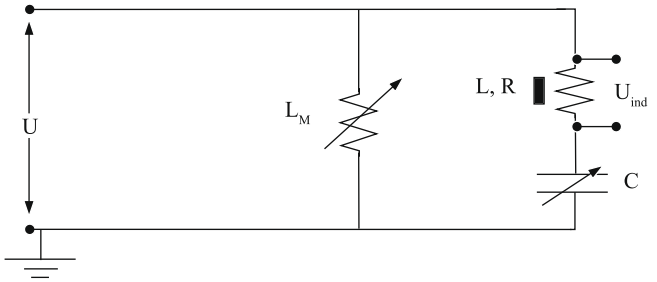

Fig. 2. Tank circuit used for the NMR experiments. Here U denotes the detected voltage, U_{ind} the (not directly detected) induction voltage, L_M the inductivity of the matching coil, C the capacity of the tuning condenser, R the resistance and L the inductivity of the NMR coil.

the excited slice would possibly not be completely located inside the RF coil. This would lead to systematically too low signal intensities for flat coils with small h.

For each flat coil, a set of four different NMR experiments was performed. As a first step, the position of the coil and the sample relative to the magnetic field was validated using a STRAFI-type 1D imaging experiments. For this, a positioning stage was scanned by means of a step motor relative to the magnetic field (see Fig. 4). At each position, the signal intensity in a Hahn echo (α -2α-) was measured. The excited slice was typically 100 μm in thickness corresponding to a pulse length of 3 μs. On the basis of the resulting STRAFI profiles the position for the further experiments was set

Table 1
Characteristic parameters of the tested flat coils. The upper table refers to RFCs the table in the middle to a SFC (see Fig. 1) and the lower one to the solenoid coil which served as reference. Here, h is the thickness (solenoid: diameter), b the width, l the length, V the sample volume, R_i the inner radius, R_a the outer radius, L the inductivity and b_1 the calculated coil coefficient. Q is the quality factor of the tank circuit embracing the particular flat coil.

	h (mm)	b (mm)	l (mm)	V (mm^3)	L (μH)	b_1 (mT/A)	Q
RFC 1	5.5 ± 0.3	6 ± 0.3	10 ± 1	140	0.27 ± 0.02	0.79	23 ± 3
RFC 2	2.5 ± 0.3	5.3 ± 0.3	10.5 ± 1	56	0.26 ± 0.02	1.3	44 ± 5
RFC 3	2.1 ± 0.3	5.9 ± 0.3	11 ± 1	28	0.32 ± 0.03	1.7	36 ± 4
RFC 4	5.8 ± 0.3	20 ± 0.3	20 ± 1	2000	0.21 ± 0.02	0.29	15 ± 2
RFC 5	2.8 ± 0.3	21.8 ± 0.3	23 ± 1	800	0.27 ± 0.02	0.44	14 ± 2
RFC 6	2.1 ± 0.3	21 ± 0.3	20 ± 1	400	0.26 ± 0.02	0.69	21 ± 3

	h (mm)	R_i (mm)	R_a (mm)	V (mm^3)	L (μH)	b_1 (mT/A)	Q
SFC	0.5 ± 0.05	2.5 ± 0.02	8.5 ± 0.02	104	0.14 ± 0.02	1.7	10 ± 1

	h (mm)	l (mm)	V (mm^3)	L (μH)	b_1 (mT/A)	Q
Solenoid	5.2 ± 0.1	10 ± 1	196	0.26 ± 0.02	1.3	23 ± 3

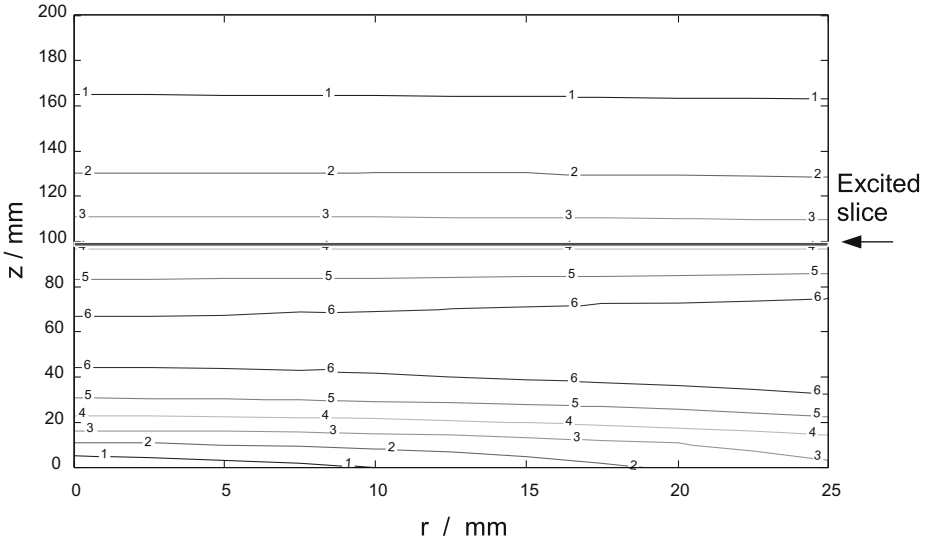

Fig. 3. Magnetic field profile of the superconducting gradient magnet used for the described experiments. Plotted is the magnetic field in T versus the distance r from the central axis and the height z relative to the center of the magnet. For $z < 0$ the magnetic field can be obtained according to $B_0(-z) = -B_0(z)$.

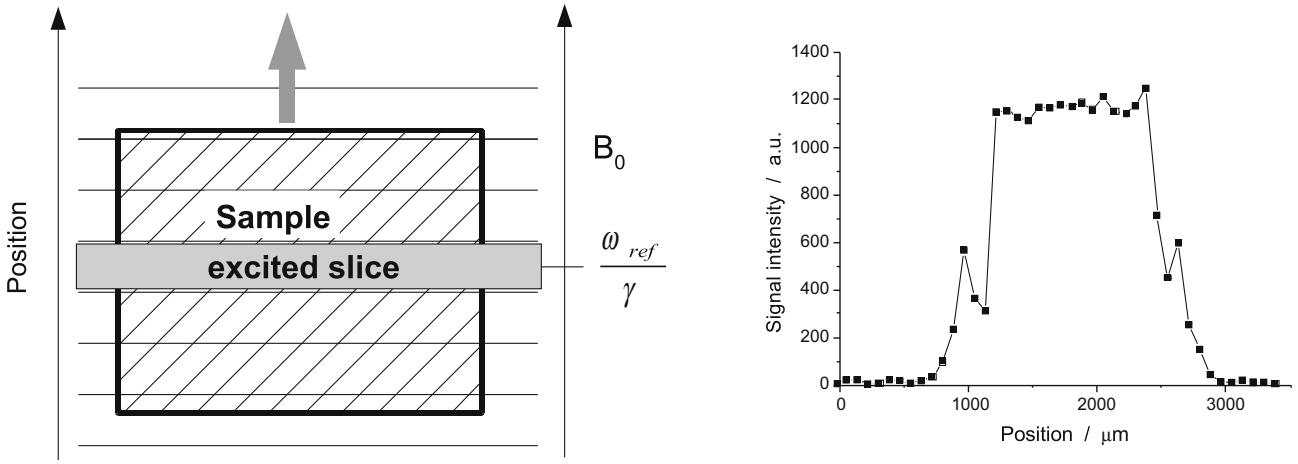

Fig. 4. Sample positioning in the magnetic field (left) for STRAFI-type profile acquisition. The gray arrow shows the direction of the movement. The horizontal lines symbolise isolines of the magnetic field B_0. The excited slice remains at the position corresponding to the reference frequency ω_{ref}. This results in a spatially resolved signal intensity profile (right). The local maxima at the edges are possibly due to a Gibbs artifact. Also glue used for sample preparation could contribute to this effect.

to the center of the profile. The following experiments were performed there:

- Optimizing of the pulse duration in Hahn echo (α -2α-) experiments at different amplifier powers: Using Hahn echos with 25 µs echo time[2] τ, the pulse length t_{PM} was determined which maximizes the signal intensity. This was done with two different amplifier powers, differing by 20 dB.
- Maximizing of the FID signal amplitude following a 20-µs-pulse. This implies that for all considered coils we compare the signal intensities of identical slice thicknesses. The signal intensity was calculated by integrating the signal amplitude over the interval from 10.5 to 12.5 µs after the pulse. This integration window is sufficiently far outside the dead time of 7 µs.

[2] Since the Hahn echo intensity $s \propto e^{-\frac{2}{3}\gamma^2 G^2 D \tau^3} \approx 0.99$ diffusion effects can be neglected.

4. Results and discussion

4.1. Comparison of theory and experiment

In Tables 2 and 3, the experimental results are compared to the calculated ones. In order to eliminate the amplification factor, the results are normalized to the signal intensity of a solenoid RF coil with circular cross-section (10 mm length, 5 mm diameter, 10 turns, $L = 0.2$ µH) and full amplifier power. For calculating the signal intensities, the actually measured coil parameters (Table 1) were used. The current during the pulse was adjusted in a way that the theoretically determined pulse lengths of maximum signal intensity t_{PM} equal the experimental ones.

In order to verify whether or not the experimental data show the expected dependence on the RF coil thickness h, they have been corrected for deviations in geometry, inductance and pulse current. The results for the RFCs are plotted in Fig. 5, together with theoretically determined signal intensities. Despite the broad scatter of the experimental data the expected dependence on h can

Table 2
Comparison of experimentally (U_{ex}) and theoretically (U_{th}) determined Hahn echo intensities. The results are given in multiples of the reference (solenoid coil, 0 dB), t_{PM} is the pulse length maximizing the signal intensity. The head line refers to the attenuation of the amplifier power.

	0 dB				20 dB			
	t_{PM} (μs)	U_{th}	U_{ex}	ΔU_{ex}	t_{PM} (μs)	U_{th}	U_{ex}	ΔU_{ex}
RFC 1	1.5	0.50	0.69	0.18	3.8	0.20	0.24	0.08
RFC 2	0.8	2.5	1.8	0.5	2.8	0.77	0.55	0.17
RFC 3	0.6	3.2	3.2	0.9	1.8	1.4	1.1	0.3
RFC 4	5	0.35	0.29	0.09	14	0.15	0.11	0.04
RFC 5	3.3	0.75	0.72	0.19	10.5	0.25	0.25	0.08
RFC 6	1.9	2.3	1.9	0.5	5.5	0.93	0.69	0.2
SFC	1.5	0.20	0.34	0.13	4.5	0.074	0.12	0.05
Solenoid	1.4	1	1	0.21	3.8	0.34	0.4	0.08

Table 3
Comparison of experimentally (U_{ex}) and theoretically (U_{th}) determined signal intensities detected directly from FID after a single pulse. The results are given in multiples of the reference (solenoid coil, Hahn echo, 0 dB), I_M is the pulse current which maximizes the signal intensity.

	I_M (A)	U_{th}	U_{ex}	ΔU_{ex}
RFC 1	1.84	0.075	0.090	0.04
RFC 2	0.66	0.21	0.13	0.05
RFC 3	0.66	0.22	0.16	0.07
RFC 5	2.6	0.25	0.23	0.08
RFC 6	1.56	0.47	0.34	0.1
SFC	1.36	0.036	0.051	0.18
Solenoid	1.36	0.13	0.13	0.02

qualitatively be observed. Additionally, the results for the solenoid coil, which served as reference, are provided.

As mentioned in Section 3, all dimensions vary by several tenths of millimeters within each coil. These variations are responsible for the major contributions to the error bar. The second important source of errors is the determination of the resonance width. Also the uncertainties in L, L_M and U contribute to the error bar of U_{ex}. In total, an error of about 20–40%, slightly increasing for small h, can

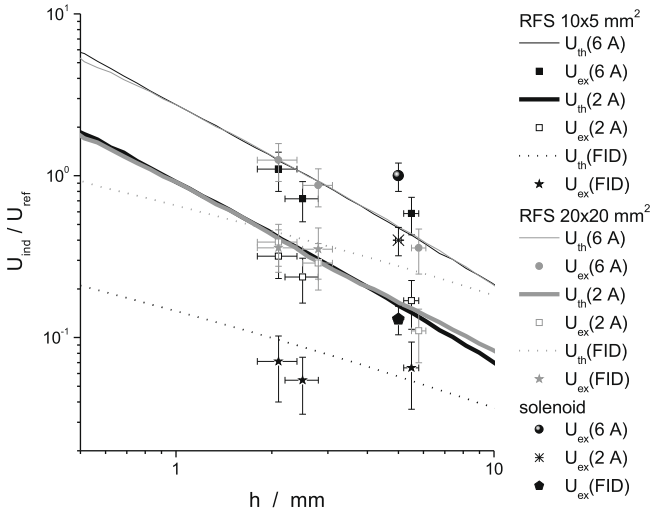

Fig. 5. Experimental (U_{ex}) and theoretical (U_{th}) signal intensities in multiples of the reference signal intensity (solenoid, pulse current 6 A) versus the RF coil thickness h. The head lines of the legends give the areas $l \times b$ of the RF coils perpendicular to the magnetic field. In brackets the pulse currents are denoted. "FID" means that the signal has been directly detected from the Free Induction Decay after a RF pulse of 20 μs length and optimized pulse current. The experimental data have been corrected to match the geometry, inductivity and amplifier power as used for determining the theoretical data.

be expected for the signal intensities. This is in agreement with the observed discrepancies between the measured and calculated signal intensities.

4.2. Theoretical optimization of flat coil geometry

After its experimental test in the previous section, Eq. (12) will now be used to optimize the flat coil geometry for given gradients. Fig. 6 shows the dependence of the RFC signal intensity on the coil geometry, the magnetic field gradient and the pulse current. For all RFCs the inductivity was set to 0.2 μH.

For small h the excited slice of a 90° pulse is broader than h. The signal intensity initially increases linearly with h, because increasingly more spins get excited. But with growing h the coil coefficient decreases and therefore t_{PM} increases. As soon as the thickness of the excited slice Δz, (which is limited by the excitation bandwidth) is smaller than h, the signal intensity again decreases. Now the number of exited spins is limited by Δz which always decreases with h. In the limit of $\Delta z \ll h$ the signal intensity is proportional to h^{-1}—the expected behavior according to the filling factor concept.

As expected, the signal intensities are generally higher for small gradients and high pulse currents. As long as the slice thickness is smaller than h the whole sample gets excited, the curves converge.

The higher the gradient and the lower the pulse current are the smaller the optimum h is. This implies that the signal enhancement due to flat coils increases with higher gradient and smaller available amplifier power.

Comparing the curves for RFCs of different surfaces $l \times b$ perpendicular to the magnetic field gradient, one observes that the curves referring to larger surfaces have their maxima at smaller h and achieve higher values. This is because the large-area flat coils produce thinner excited slices for the same pulse current due to lower b_1. But due to their larger surface $l \times b$ they yield approximately the same signal intensity for $\Delta z \ll h$. Because of their lower coil coefficient the maximum is reached for smaller h. There, the signal intensity is higher because the number of excited spins is only limited by the sample size.

A slightly different behavior is shown by the signal intensities detected directly from FID following a single pulse (Fig. 7). In contrast to the echo studies shown in Fig. 6 the pulse current, not the pulse length was optimized in these simulations. The pulse length was fixed to 20 μs, therefore also Δz was constant. Like that, the signal intensity in the limit of $\Delta z \ll h$ exhibits a decrease proportional to $1/\sqrt{h}$. For small coil thicknesses $h < \Delta z$, by contrast, the curves converge and follow the same dependence as the signal intensity in a homogeneous field.

In contrast to the Hahn echo experiments the position of the intensity maxima is not dependent on the coil surface since a fixed pulse length was used. Under these conditions, an increasing coil surface just leads to a shift of the curves to higher values.

5. Discussion

The results of the previous subsection suggest that the sensitivity of SFG NMR echo experiments can be dramatically increased by using flat coils. Especially for highest static gradients, where SNR problems are most pronounced, flat coils offer their most significant enhancement potential. However, it is technically quite demanding to manufacture very thin RFCs with the required precision. In this case, SFCs offer an interesting alternative, since their automated production by means of photolithographic techniques is quite straightforward. Additionally, SFCs bear the potential to solve a specific problem of applying flat coils even in the region of maximal gradient strength in an

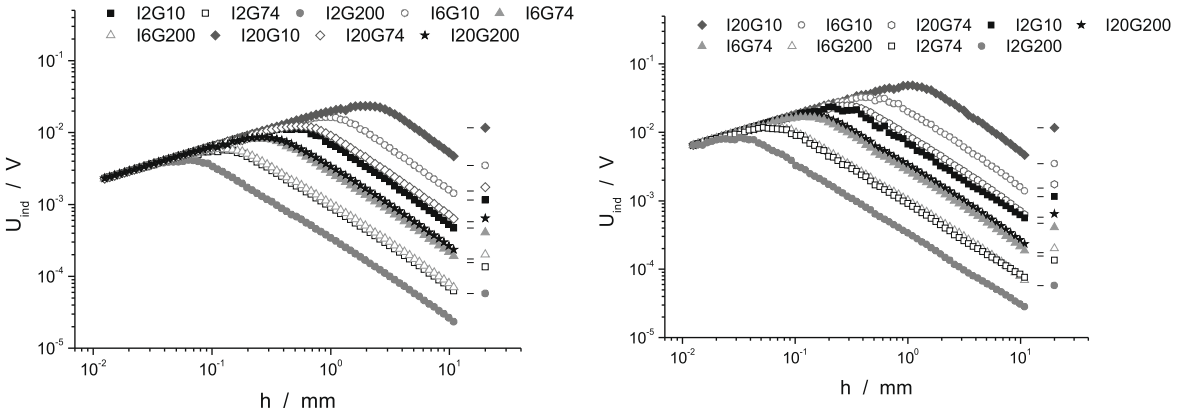

Fig. 6. Calculated Hahn echo intensities for RFCs depending on their thickness h. The left plot refers to RFCs with $l \times b$ = 10 mm × 5 mm perpendicular to the magnetic field gradient and the right plot to such with $l \times b$ = 20 mm × 20 mm. The assignment convention for the curves used in the legends is I[pulse current in A]G[gradient in T/m]. Only spins with Larmor frequencies differing from the reference frequency by less than 1.9 MHz have been considered. The short stripes mark the signal intensities of the solenoid reference coil (L = 0.2 μH, 5 mm diameter, 10 mm length) corresponding to the symbol on the right.

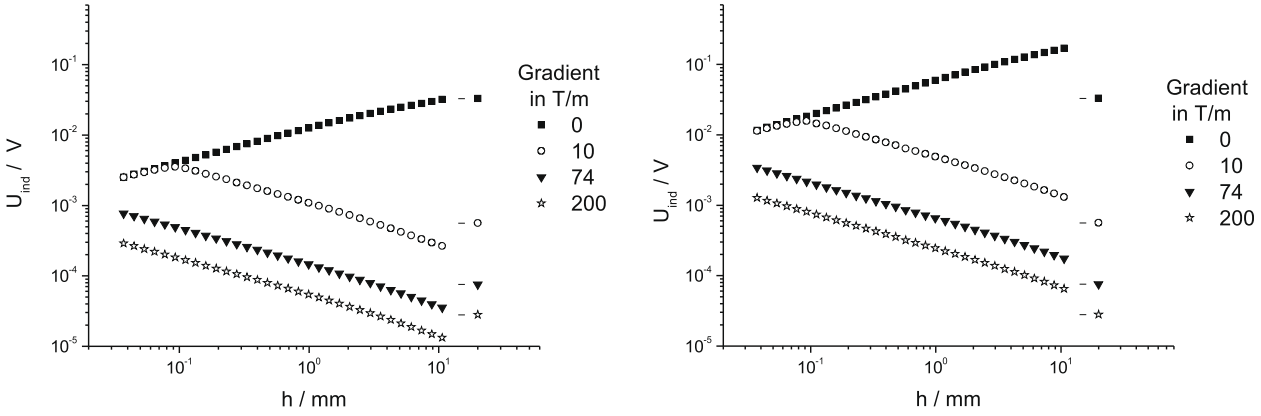

Fig. 7. Calculated signal intensities of RFCs, detected 10.5 μs after a RF pulse of 20 μs length. The left plot refers to RFCs with an area $l \times b$ = 10 mm × 5 mm perpendicular to the magnetic field gradient and the right plot to ones with $l \times$ b = 20 mm × 20 mm. Only spins with Larmor frequencies of 20 kHz around the reference frequency have been considered. The short stripes mark the signal intensities of the solenoid reference coil (L = 0.2 μH, 5 mm diameter, 10 mm length) corresponding to the symbol on the right.

anti-Helmholtz dedicated gradient magnet. In such magnets, the field isolines in the zone of the strongest gradient are quite strongly curved. SFCs could possibly be formed in a way that they exhibit exactly the same curvature.

Also for stray field imaging flat RF coils offer an enhancement of the SNR, or alternatively of the spatial resolution. Referring to our results, for microimaging experiments it is attractive to detect the signal directly from the FID since the signal intensity is much higher than that from a Hahn echo experiment providing the same spatial resolution. Considering that the $SNR \propto 1/\sqrt{\Delta f}$ increases with decreasing spectral width Δf, signal detection directly from FID becomes even more attractive. In the case of gradients, typical for the stray field of superconducting magnets, the optimum h is in the order of micrometers. Therefore SFCs may allow obtaining NMR profile images of micrometer layers with a resolution in the far sub-micrometer range perpendicular to the layer direction.

Further advantageous properties of flat coils in SFG NMR are

- the smaller amounts of samples (a few mg instead of a few 100 mg loading in a conventional solenoidal coil) needed for the experiments and
- the possibility to conduct experiments at lower pulse power (which eliminates the need for expensive power amplifiers in the kW range).

6. Summary

In this work, it has been shown, experimentally and theoretically, that flat coils can serve to enhance the sensitivity of SFG NMR experiments. An equation for the NMR signal density has been derived from Bloch equations and numerically integrated. It has been experimentally validated by comparing the experimentally determined and calculated signal intensities of seven flat coils at different pulse sequences and pulse currents. Six of seven flat coils were rectangular flat coils (RFC) and one a spiral flat coil (SFC). SFCs have the advantage that they can be produced using standard lithographical techniques which allow high precision even at low thicknesses.

Additionally, the expression for the signal density has been used to study the dependence of the signal intensity on the coil geometry, the magnetic field gradient and the pulse current. In the limit of large coil thicknesses h the signal is proportional to h^{-1}, in the case of fixed pulse length proportional to $h^{-1/2}$.

The higher the gradient and the lower the amplifier power the higher the potential of flat coils is to enhance the signal intensity.

Another important result of this work is that detecting the signal directly from FID is particularly interesting for microimaging experiments.

Indeed, we already used this method for microimaging experiments on heavy ion irradiated crystals [23,24]. Moreover, we used

flat coils for conventional NMR diffusion measurements on PDMS and for studying diffusion effects in thin slices [25].

References

[1] Marinus T. Vlaardingerbroek, Jacques A. Den Boer, Magnetic Resonance Imaging, Springer, 1996.
[2] Kärger F. Stallmach, J. Kärger, The potentials of pulsed field gradient NMR for investigation of porous media, Adsorption 5 (1999) 117–133.
[3] W.S. Price, Pulsed-field gradient nuclear magnetic resonance: basic, Concepts Magn. Reson. 9 (1997) 299–336.
[4] W.S. Price, Pulsed-field gradient nuclear magnetic resonance: experimental, Concepts Magn. Reson. 10 (1998) 197–237.
[5] E.O. Stejskal, J.E. Tanner, Spin diffusion measurements: spin echoes in the presence of a time-dependent field-gradient, J. Chem. Phys. 42 (1965) 288–292.
[6] J.E. Tanner, E.O. Stejskal, Restricted self-diffusion of protons in colloidal systems by the pulsed-gradient, spin–echo-method, J. Chem. Phys. 49 (1968) 1768–1777.
[7] J.E. Tanner, Use of stimulated echo in NMR diffusion studies, J. Chem. Phys. 52 (1970) 2523–2526.
[8] A. Gutsze, W. Masierak, B. Geil, D. Kruk, H. Pahlke, F. Fujara, On the problem of field-gradient NMR measurements of intracrystalline diffusion in small crystallites—water in NaA zeolites as an example, Solid State Nucl. Magn. Reson. 28 (2005) 244–249.
[9] R. Kimmich, NMR: Tomography, Diffusometry, Relaxometry, Springer, 1997.
[10] I. Chang, F. Fujara, B. Geil, G. Hinze, H. Sillescu, A. Tölle, New perspectives of NMR in ultrahigh static magnetic field gradients, J. Non-Cryst. Solids 172–174 (1994) 674–681.
[11] B. Geil, Measurement of translational molecular diffusion using ultrahigh magnetic field gradient NMR, Concepts Magn. Reson. 10 (5) (1998) 299.
[12] A.A. Samoilenko, D.Y. Artemov, L.A. Siebeldina, Formation of sensitive layer in experiments on NMR subsurface imaging of solids, JETP Lett. 47 (1988) 417–419.
[13] E.W. Randall, Advances in NMR, in: D.M. Grant, R.K. Harris (Eds.), The Encyclopedia of Nuclear Magnetic Resonance, vol. 9, John Wiley and Sons, 2002, pp. 150–164.
[14] P.J. MacDonald, Stray field magnetic resonance imaging, Prog. Nucl. Magn. Reson. Spectrosc. 30 (1997) 69–99.
[15] P.M. Glover, P.S. Aptaker, J.R. Bowler, E. Ciampi, P.J. McDonald, A novel high gradient permanent magnet for the imaging of planar thin films, J. Magn. Res. 139 (1999) 90–97.
[16] B. Bechinger, S.J. Opella, Flat-coil probe for NMR spectroscopy of oriented membrane samples, J. Magn. Res. 95 (1991) 585–588.
[17] J.K. Rainey, J.S. DeVries, B.D. Sykes, A rotatable flat coil for static solid-state nuclear magnetic resonance spectroscopy, Rev. Sci. Instr. 76 (2005) 086102.
[18] F. Bălibanu, Kidist Hailu, R. Eymael, D.E.. Demco, B. Blümich, Nuclear magnetic resonance in inhomogeneous magnetic fields, J. Magn. Res. 145 (2000) 246–258.
[19] D.I. Hoult, The principle of reciprocity in signal strength calculations—a mathematical guide, Concepts Magn. Res. 12 (4) (2000) 173–187.
[20] F. Bloch, Dynamical Theory of Nuclear Induction. II, Phys. Rev. 102 (1956) 104–135.
[21] Mathematica 4 for students. Available from: www.wolfram.com.
[22] W. Gander, W. Gautschi, Adaptive Quadrature—Revisited, BIT, 40 (2000) 84, implemented in Matlab 7.4.0.287 (R2007a).
[23] H. Stork, A. Hamburger, A. Gädke, F. Fujara, K. Schwartz, Spatially resolved characterization of heavy ion irradiated crystals using static field gradient nuclear magnetic resonance, J. Phys. Condens. Matter 20 (2008) 275236.
[24] H. Stork, K.-P. Dinse, F. Fujara, A. Hamburger, P. Jakes, R. Neumann, K. Schwartz, C. Trautmann, Spatially resolved characterization of Xe ion irradiated LiF crystals using static field gradient NMR, J. Phys. Condens. Matter 20 (2008) 465215.
[25] A. Gädke, N. Nestle, Apparent longitudinal relaxation of mobile spins in thin, periodically excited slices, Diffusion Fundam. 3 (2005) 38.1–38.12.